Materials Performance and Characterization

doi:10.1520/MPC20170083 / Vol. 7 / No. 4 / 2018 / available online at www.astm.org

Tuomas Jokiaho,[1] Suvi Santa-aho,[2] Henri Järvinen,[2] Mari Honkanen,[2] Pasi Peura,[2] and Minnamari Vippola[2]

Effect of Microstructural Characteristics of Thick Steel Plates on Residual Stress Formation and Cracking during Flame Cutting

Reference

Jokiaho, T., Santa-aho, S., Järvinen, H., Honkanen, M., Peura, P., and Vippola, M., "Effect of Microstructural Characteristics of Thick Steel Plates on Residual Stress Formation and Cracking during Flame Cutting," *Materials Performance and Characterization*, Vol. 7, No. 4, 2018, pp. 655–674, https://doi.org/10.1520/MPC20170083. ISSN 2379-1365

ABSTRACT

Thick wear-resistant steel plates are commonly used in demanding conditions, such as in the mining industry. In harsh environments, a high degree of both toughness and hardness is required, which extends the service life of the components but also makes the production of the plates difficult. Flame cutting is a generally applied cutting method in the heavy steel industry since it enables the cutting of thick steel plates at high production rates. However, flame cutting may cause cracks in the cut edge of the steel plates, leading to rejects for the steel industry and end-users. In addition, cutting generates a heat-affected zone at the cut edge, where volumetric and microstructural changes and hardness variations take place. A steep thermal gradient, generated during flame cutting, also produces high residual stresses on the cut edge. The goal of this study is to examine how microstructural features contribute to the residual stress formation and cracking probability of thick steel plates. Specific microstructural features can make the plates prone to cracking and tend to produce undesired stresses during the cutting process. The residual stress profiles of flame-cut specimens were measured using the X-ray diffraction method. In addition, the mechanical properties of steel plates were evaluated. The microstructures of the cut edge and the base material were characterized by electron microscopy. Results indicate that the shape of the prior austenite grains has an effect on both the cracking probability and residual stress

Manuscript received June 22, 2017; accepted for publication January 4, 2018; published online June 7, 2018.

[1] Tampere University of Technology, Laboratory of Materials Science, P.O. Box 589, FI-33101 Tampere, Finland (Corresponding author), e-mail: tuomas.jokiaho@tut.fi, https://orcid.org/0000-0002-6419-0582

[2] Tampere University of Technology, Laboratory of Materials Science, P.O. Box 589, FI-33101 Tampere, Finland https://orcid.org/0000-0002-0047-3268 (S.S.-A.)

formation. Longitudinally oriented prior austenite grain boundaries combined with a high residual tensile stress state provide potential sites for cracking.

Keywords

flame cutting, microstructure, residual stress, heat-affected zone, thick steel plate, X-ray diffractometer, electron microscopy

Introduction

High hardness and toughness are required for thick wear-resistant steel plates, but these properties are what make manufacturing difficult. Mechanical cutting of the plates is demanding and slow because the plates are almost as hard as the cutting tools. For this reason, thermal cutting methods are preferred. Flame cutting especially is a generally applied method in the steel industry for thick and wear-resistant plates. In addition, flame cutting is an exothermal process that generates large amounts of heat during the cutting process, which supports the continuum of the cutting process. Therefore, it enables the cutting of very thick plates and creates a major advantage compared to other thermal cutting methods [1].

The flame cutting process begins with heating a small area on the steel surface up to its ignition temperature using an oxyfuel gas flame. A jet of pure oxygen is then directed to the locally heated area, which causes rapid burning of the heated metal, thus creating a cut edge. In addition, the oxygen jet flushes the molten iron oxide away from the cut edge and exposes clean surfaces for cutting [2]. Consequently, a heat-affected zone (HAZ) is generated at the cut edge of the steel plate that is due to the formation of large thermal gradients during the flame cutting process. Martín-Meizoso et al. [3] reported that flame cutting of a 25-mm-thick steel plate produced higher hardness values near the cut edge that subsequently decreased toward the base material. Wilson [4] investigated thermal cutting of steel plates with thicknesses of 25.4, 50.8, and 101.6 mm, and it was shown that faster cutting speeds produced a narrower HAZ with higher hardness levels. In addition, richer chemistry steel plates tended to have broader and harder HAZ. Wood [5] noticed that flame cutting of 25-mm-thick low-carbon and low-alloy steel plates produced highest hardness close to the cut edge and decreased the hardness values toward the base material. The maximum hardness increased with faster cutting speeds [5]. High temperature and fast cooling during cutting produced a martensitic layer on the cut edge, which was followed by a region of tempered martensite [5]. As a common finding, hardness variations and microstructural changes take place in the HAZ, and it was noted in all studies that the hardness was greater near the cut edge and decreased toward the base material.

However, flame cutting may cause cracks in the cut edge of the steel plate. The size of the cracks can vary from micrometers to several centimeters. Generally, cracks are formed horizontally near the centerline of the steel plate, but cracks can also propagate in the vertical direction. The cracking tendency has been noticed to increase as the hardness and thickness of the steel increase [6]. In addition, flame cutting produces residual stresses (RSs) at the cut edge of the steel plate, and it has been reported [7] that high residual tensile stresses promote crack formation. RSs are internal stresses inside the material, and they are present even after all external forces have been removed. RSs originate from local misfits of the material, i.e., nonuniform plastic deformation that causes elastic strains to maintain

dimensional continuum [8]. In the case of flame cutting, the RSs can be divided into thermal stresses and transformation stresses. Thermal stresses arise from different thermal expansions and contractions of material during heating and cooling. Transformation stresses, in turn, arise from variations in volumetric sizes of different phases and microconstituents. [9]

RSs are often divided into three types (I, II, III) according to the scale over which they impact and self-equilibrate. Type I is a macrostress, which varies over large distances. This long-range stress is often referred to as the most important one because it equilibrates over a macroscopic distance, such as the scale of a structure. In contrast, Types II and III are microstresses, which vary in microscopic scale, thus making their influence difficult to predict. Type II stresses vary over the grain scale and nearly always exist in polycrystalline structures when the elastic and thermal properties are different between differently oriented neighboring grains. Type III stresses exist on atomic scale and are balanced within a grain, such as, for example, those stresses caused by dislocations and point defects. The measuring method has to be carefully considered as it depends on the stress type that is being measured. Typically, most material removal methods, i.e., hole drilling, measure only Type I stresses, as Types II and III stresses are averaged to zero in the sampled area. In diffraction-based measuring methods, the stress value is derived from a specific wavelength and diffraction condition. Therefore, the particular phase or grain orientation is sampled, and Type II stress can be recorded as superimposed on the Type I stress. [8]

Previous studies have been mainly focused on the modeling of RSs, and the simulation results have been verified by experimental measurements. Lindgren, Carlestam, and Jonsson [7] investigated and simulated the RS formation in the thermal cutting of thick steel plates. It was noticed that cutting produced a compressive stress area near the cut edge, and there was a tensile stress peak after the compressive stress region. RS values could be affected by changing the cutting parameters; for example, preheating produced more compressive stress and also lowered the tensile stress peak. Similar results were found in earlier studies [10,11] by the current author; the RS state was affected by the size of the specimen and cutting parameters. Preheating not only lowered the tensile stress but also increased the compressive stress area by shifting the tensile stress peak deeper in the subsurface. However, there is still a lack of knowledge on how RSs and crack formations are affected, e.g., by microstructural features. The aim of this study is to investigate the effect of microstructures on the RS formation and cracking probability and to identify the most suitable microstructural features from the flame cutting point of view.

Materials and Methods

The experimental procedure for understanding the effect of microstructural characteristics on RS and crack formation is presented schematically in **Fig. 1**. Firstly, the initial mechanical properties and microstructure of the studied steels (A and B) were examined. Then the steel plates were flame cut using different cutting speeds (150, 300, and 500 mm/min) and ultrasonically inspected after the cutting. After the ultrasonic inspection, the RSs were measured from the flame-cut specimens. The measured specimens were then sectioned for hardness measurements, electron microscopy analysis (SEM, transmission electron microscope (TEM)), and glow discharge optical emission spectroscopy (GDOES) measurements. Each of these experimental steps are described more precisely in the Materials and Experimental Procedure sections.

FIG. 1

Experimental procedure of the study.

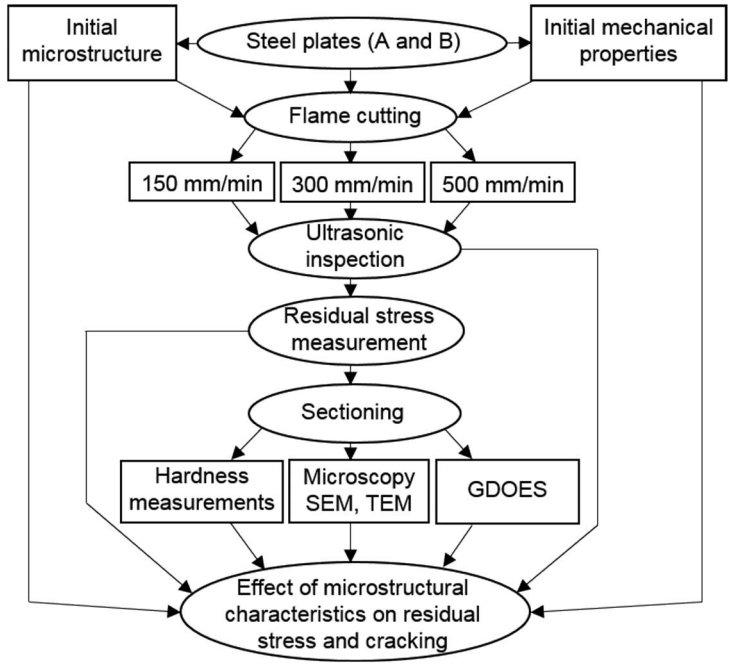

TABLE 1

Composition of studied steel types A and B.

Steel Plates	C %	Si %	Mn %	Cr %	B %	Mo %	Al %	Ni %	V %	Ti %
A	0.15	0.62	1.10	0.62	0.0015	0.42	0.048	0.20	0.042	0.017
B	0.14	0.55	1.05	0.57	0.0012	0.36	0.044	0.19	0.039	0.013

MATERIALS

The materials examined were hot-rolled, wear-resistant steel plates (A and B), of which steel plate A had a higher hot-rolling temperature (above 900°C) than steel plate B (below 900°C). The compositions of the studied steels are presented in Table 1. The dimension of the flame-cut specimens were 40 by 150 by 150 mm (thickness by width by length), and one side of each specimen was cut with an oxyfuel propane gas flame. The cutting speeds used for the specimens were 150, 300, and 500 mm/min, and the specimens were inspected using Phasor XS 16/16 Olympus ultrasonic equipment (General Electric, Boston, MA) with an MSEB 4 dual probe (4 MHz) after flame cutting. Ultrasonic inspection results were verified by repeating the inspections with two individual researchers and by sectioning a few specimens after inspection to confirm the existence of the defects.

EXPERIMENTAL PROCEDURE

The X-ray diffraction method (XRD) was used to measure the RSs from the flame-cut specimens. The measurement equipment was XStress 3000 (Stresstech Oy, Jyväskylä, Finland) and the measurement method used was the modified Chi method [12]. The principle of the method is the calculation of the interplanar lattice spacing of the ferrite [211]

plane from the 156° Bragg diffraction angle. Different Ψ tilts are used to measure the lattice spacing d (where the Ψ angle is the angle between the normal of the specimen and the normal with the diffracting plane). The RS can be calculated using the elastic properties of the material and the slope from a plot of measured lattice spacing d as a function of $\sin^2 \Psi$. Thus, RS can be calculated from a specific measurement location by using the following equation and [13]:

$$\sigma_\phi = \left(\frac{E}{1+\upsilon}\right) m \tag{1}$$

where σ_ϕ is the RS in the measurement direction ϕ, E is the Young's modulus, ν is Poisson's ratio, and m is the gradient of the measured d versus $\sin^2\Psi$ curve. The steeper the gradient m, the higher the RS level. The measurement parameters used are presented in Table 2.

RS measurements were performed at the centerline of the specimens, where the cracks are mostly formed during flame cutting. Measurements were carried out in two perpendicular measurement directions, 0° and 90°, which correspond to the cut direction and to the thickness direction of the specimen, respectively. The chosen directions are the most critical orientations for crack formation. The measurement locations and directions are shown in Fig. 2a.

An exposure time of 5 seconds was used in each RS measurement. To produce the RS depth profiles, the material layers were removed from the measurement location with an electrolytic polishing machine, Movipol-3 (Struers Inc., Cleveland, OH). The electrolyte used in polishing was A2 (60 % perchloric acid, 65–85 % ethanol, 10–15 % 2-butoxyethanol, and 5–15 % water). The removed material depths were approximately 100–200 μm between each measurement, and each polishing step was verified with a digital dial indicator. An example of the measured RS profile is presented in Fig. 3.

TABLE 2

Measurement parameters used for XStress 3000.

Parameter	Value/Unit	Parameter:	Value/Unit
ϕ rotations (measurement directions)	0° and 90°	Modulus of elasticity	211 GPa
Collimator	3 mm	Poisson's ratio	0.3
ψ tilt angles in one direction (side / side)	6 / 6	Voltage	30 kV
Maximum tilt angle	40°	Current	6.7 mA
ψ oscillation	5°	Radiation	CrKα

FIG. 2

(a) RS measurement location and directions and (b) hardness profile location.

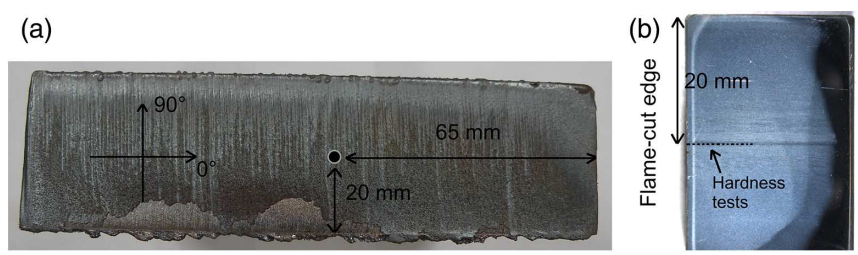

FIG. 3

RS profile from flame-cut specimen. RS and full width at half maximum in flame-cut direction (0°) and thickness direction (90°).

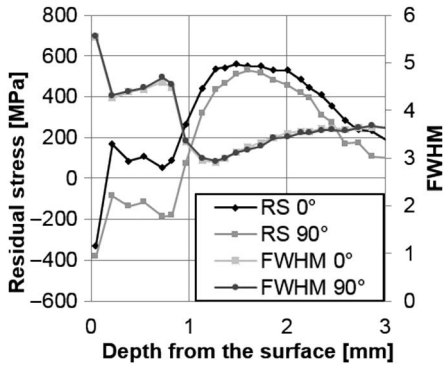

RS profiles include RSs and full width at half maximum values in both the flame-cut and thickness direction. However, as most of the cracks are formed in the flame-cut direction, the most critical RSs for crack formation are the ones formed in the thickness direction (90°) of the plates. For this reason, this study concentrates on the RS formation in the thickness direction of the plate.

Flame-cut specimens were sectioned from the centerline for microstructural analysis, which was carried out using scanning electron microscopes (SEMs). For microstructural analysis and hardness measurements, the specimens were ground using abrasive silicon carbide papers and polished with 3 and 1-μm diamond suspensions. After grinding, the specimens were etched with 4 % Nital solution. Hardness measurements of the original structure (HV 5 kg) were carried out using a DuraScan 80 (Struers Inc., Cleveland, OH) and the cross-section hardness profiles (HV 0.2 kg) from the flame-cut edge were performed with a MMT-X7 digital microhardness tester (Matsuzawa, Akita, Japan). The location of the hardness tests in relation to the flame-cut edge is presented in **Fig. 2b**. Tensile tests in the thickness direction were carried out with an MTS 250 kN and tests were performed according to SFS-EN ISO 6892-1, *Metallic Materials—Tensile Testing—Part 1: Method of Test at Room Temperature* [14]. In addition, GDOES profiles were measured from the flame-cut surfaces with a GDA 750/GDA 550 spectrometer (Spectruma Analytik GmbH, Hof, Germany). The microstructure characterization was carried out using a Philips XL-30 SEM (SEMTech Solutions, Billerica, MA) and an ULTRAplus field emission SEM (ZEISS, Oberkochen, Germany).

In addition, the specimens were analyzed in SEM with an HKL Premium-F Channel Electron Backscatter Diffraction (EBSD) system equipped with a Nordlys F400 detector (Oxford Instruments, Abingdon, United Kingdom). The specimens used in the EBSD measurements were sectioned and ground using abrasive silicon carbide paper and then polished with a colloidal silica suspension (0.04 μm). A step size of 0.1 μm and an acceleration voltage of 20 kV were used in the EBSD analysis of cross-sectional areas measuring 209 by 144 μm. The EBSD data obtained from the original microstructure was used as a starting point for reconstructing the grain boundaries of the prior austenite. The reconstruction was carried out using a MATLAB-based (MathWorks, Natick, MA) iterative algorithm originally developed by Nyyssönen et al. [15]. The algorithm determines an experimental orientation relationship between martensite and prior austenite and uses that information to reconstruct the grain boundaries of prior austenite. The script used was

supplemented with the MTEX texture and crystallographic analysis toolbox developed by Bachmann, Hielscher, and Schaeben [16]. A map revealing the grain boundaries was assembled from the EBSD orientation pixel map by using MTEX as described in Ref. [15]. A minimum grain boundary threshold value of 8° was applied. The prior austenite grain sizes (PAGS) were then measured from the reconstructed grain boundary maps by mean linear intercept.

A JEM-2010 TEM (Jeol Ltd., Tokyo, Japan) equipped with a Noran Vantage Si(Li) detector energy dispersive spectrometer (EDS; Thermo Fisher Scientific Inc., Raleigh, NC) was used to analyze precipitates before and after flame cutting. The TEM specimens were prepared using an extraction replica technique: the sectioned specimen was polished by a traditional metallographic method followed by etching (Nital 4 % solution) to remove the matrix so that the precipitates stood proud of the specimen surface. Then, a carbon film was evaporated on the specimen surface and scored into ~1 mm^2. After this, etching continued to dissolve the matrix and the squares of the carbon film carrying the precipitates with them were floated in distilled water and collected on copper TEM grids.

Results

SEM micrographs from the centerline of steel specimens A and B are presented in Fig. 4. The original structure of the specimens consists mainly of lath martensite (M, shown in Fig. 4). However, both microstructures may also contain a small amount of bainite (B, shown in Fig. 4), which is often difficult to distinguish from a martensite structure.

Some of the prior austenite grains can be distinguished in steel specimens A and B. However, the martensite and prior austenite grain structures are difficult to evaluate and compare from the SEM micrographs. For further investigation, an EBSD analysis was made for both steels, and the prior austenite grain boundaries (PAGBs) were constructed as previously described. The reconstructed PAGBs from the original microstructures of specimens A and B are presented in Fig. 5.

EBSD analysis and reconstruction of the prior austenite grains were used to calculate the PAGS and to evaluate the microstructures of the specimens using an 8° minimum grain boundary threshold. The PAGS of specimens A (Fig. 5a) and B (Fig. 5b) are 53 μm and 34 μm, respectively. Steel A has equiaxed prior austenite grains with few packet boundaries inside the grains. In contrast, the prior austenite grains in Steel B are elongated

FIG. 4 SEM micrographs of steel specimens (a) A and (b) B. Arrows indicate examples of martensite (M) and bainite (B).

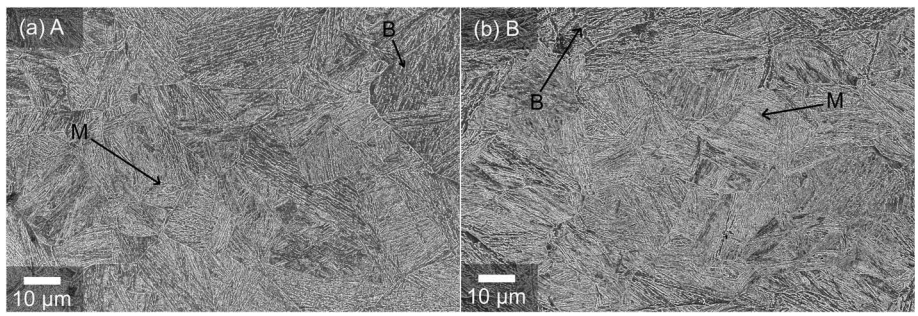

FIG. 5 Reconstructed PAGB maps for specimens (a) A and (b) B. PAGBs are superimposed on EBSD band contrast images as black lines. The red and green lines show the packet and block boundaries of martensite, respectively. (For interpretation of the references to color in these figures, the reader is referred to the web version of this article.)

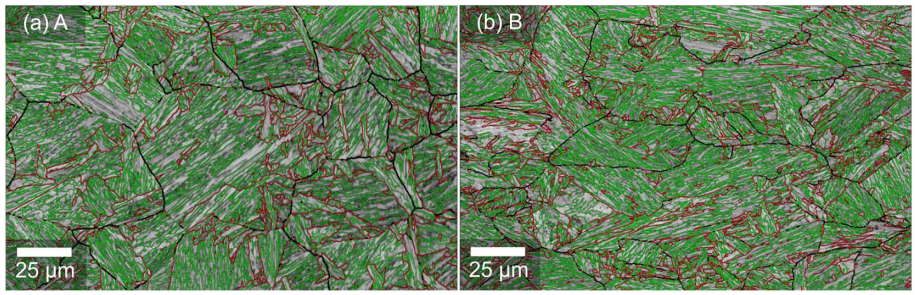

TABLE 3

Initial mechanical properties for Steels A and B. Tensile strength (R_m) corresponding to the maximum force and reduction of the area at fracture (Z %) in tensile tests. PAGS is expressed as the mean linear intercept (L_m) calculated from EPSD data.

Steel Grade	Hardness (HV 5kg)	R_m (MPa)	Z %	PAGS L_m (μm)
A	399	1,217	51	53
B	414	1,184	53	34

in the horizontal direction with more packet boundaries. In addition, Steel B has more block boundaries and a denser martensitic block structure compared to Steel A.

The initial mechanical properties of Steels A and B were tested by means of hardness measurements and tensile tests. The results presented in Table 3 show that there is only a small variation in hardness values and tensile properties between Steels A and B. To summarize, the mechanical properties of the original structures are similar for both steels. However, as noted previously, significant differences were observed in their microstructural features, especially in the prior austenite grain morphologies of Steels A and B.

FLAME CUTTING EXPERIMENTS

Steel specimens A and B were flame cut using three different cutting speeds: 150, 300, and 500 mm/min. Microstructural characterization showed that all the tested flame cutting speeds created a HAZ at the cut edge of the steel plate. In addition, three distinct microstructural regions (presented in Fig. 6) were identified from the HAZ in all the studied specimens a newly formed martensite region, a two-phase region, and the tempered original structure.

These regions have typical features that are present in all the studied flame-cut specimens. The region closest to the cut edge is fully austenized during the flame cutting and transforms into martensite during rapid cooling. An example micrograph of the martensite region formed close to the cut edge is presented in Fig. 7. The martensite region near the cut edge consists of martensite laths and autotempered martensite regions (indicated by arrows in Fig. 7), containing acicular-shaped cementite (Fe_3C) particles [17]. Martensite transformation occurs between the martensite start (M_s) and martensite finish (M_f) temperatures, which depend on the carbon content and alloying of the steel.

FIG. 6 SEM micrograph of the HAZ showing the newly formed martensite (1.), two-phase region (2.), and tempered original structure (3.).

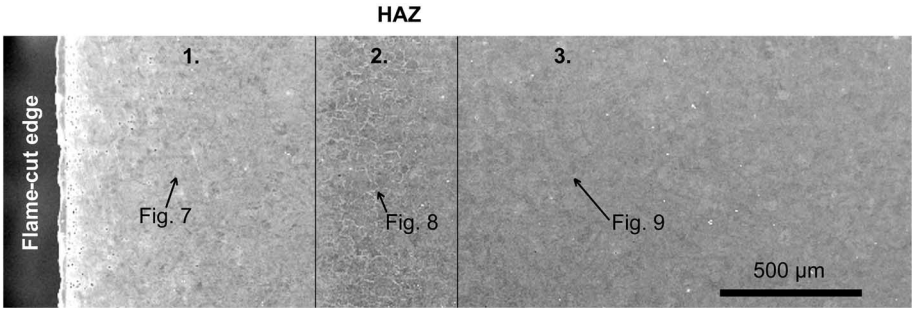

FIG. 7

SEM micrograph of a newly formed martensite region close to the cut edge. This region consists of a mixture of martensite laths and autotempered martensite (indicated by arrows) containing acicular-shaped Fe_3C.

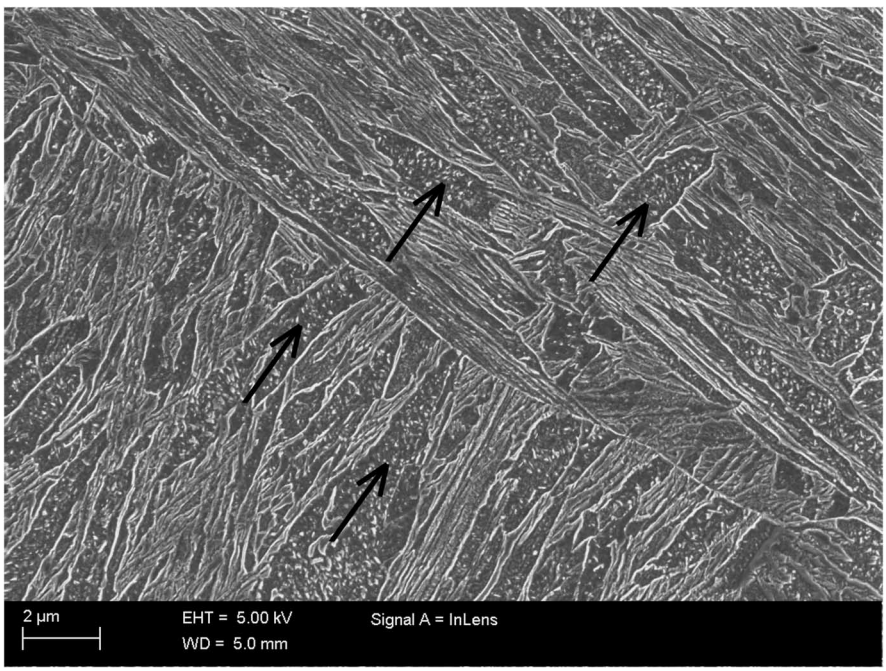

Therefore, the martensite that formed close to the M_s temperature is exposed to tempering conditions during the remaining quench cycle, which is called autotempering. The effect of autotempering increases with lower carbon content (lower carbon steels have a higher M_s) and a reduction in quench severity (increasing the time that fresh martensite is exposed to elevated temperatures) [18].

After the newly formed martensite, there is a two-phase region, which is a mixture of newly formed martensite and tempered original structure. An example structure of the two-phase region is presented in Fig. 8. The two-phase region is partly austenized during flame cutting and the austenization occurs heterogeneously at the PAGBs, while the rest of the structure is heavily tempered. During cooling, austenite forms a fine martensite lath

FIG. 8

SEM micrograph of the two-phase region containing both newly formed martensite and tempered original structure.

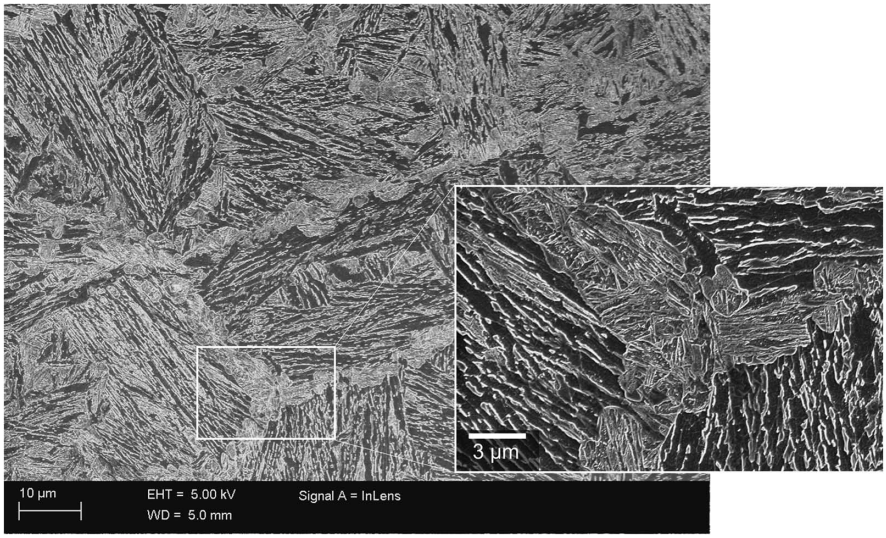

structure, which creates martensitic chains in the PAGBs while the original structure inside the prior austenite grains is tempered.

After the two-phase region, there is the tempered original structure, which is presented in Fig. 9. The original structure is the most tempered in the two-phase region that undergoes the highest temperatures during flame cutting without austenizing. The tempering effect

FIG. 9

SEM micrograph of tempered original structure containing fine dispersed Fe_3C particles (white dots).

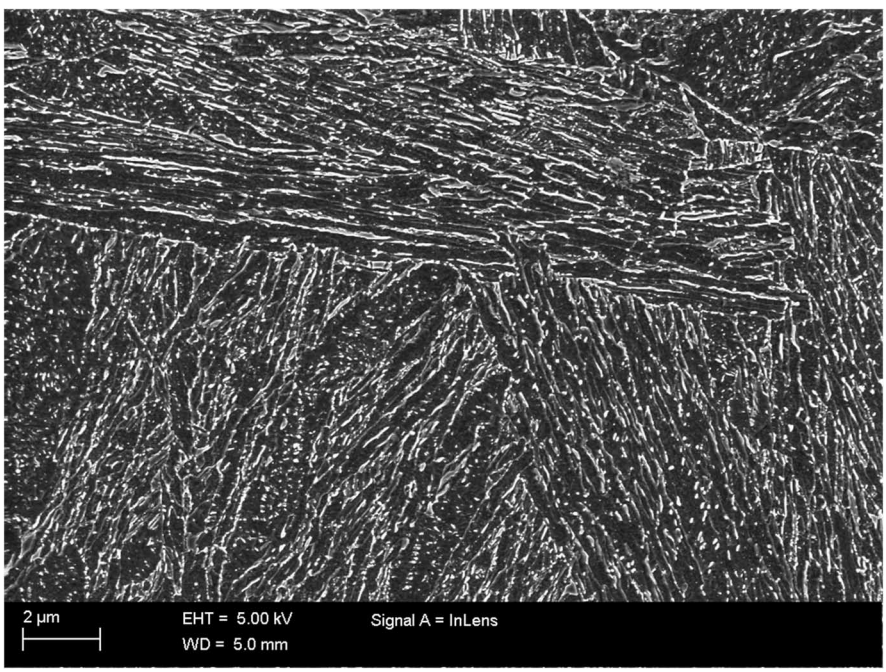

FIG. 10 Microstructural regions of the cut edge (newly formed martensite (1.), two-phase region (2.), and tempered region (3.)) from specimens A and B after 150, 300, and 500 mm/min of flame cutting. The measured RS profiles in the thickness direction are represented for each specimen.

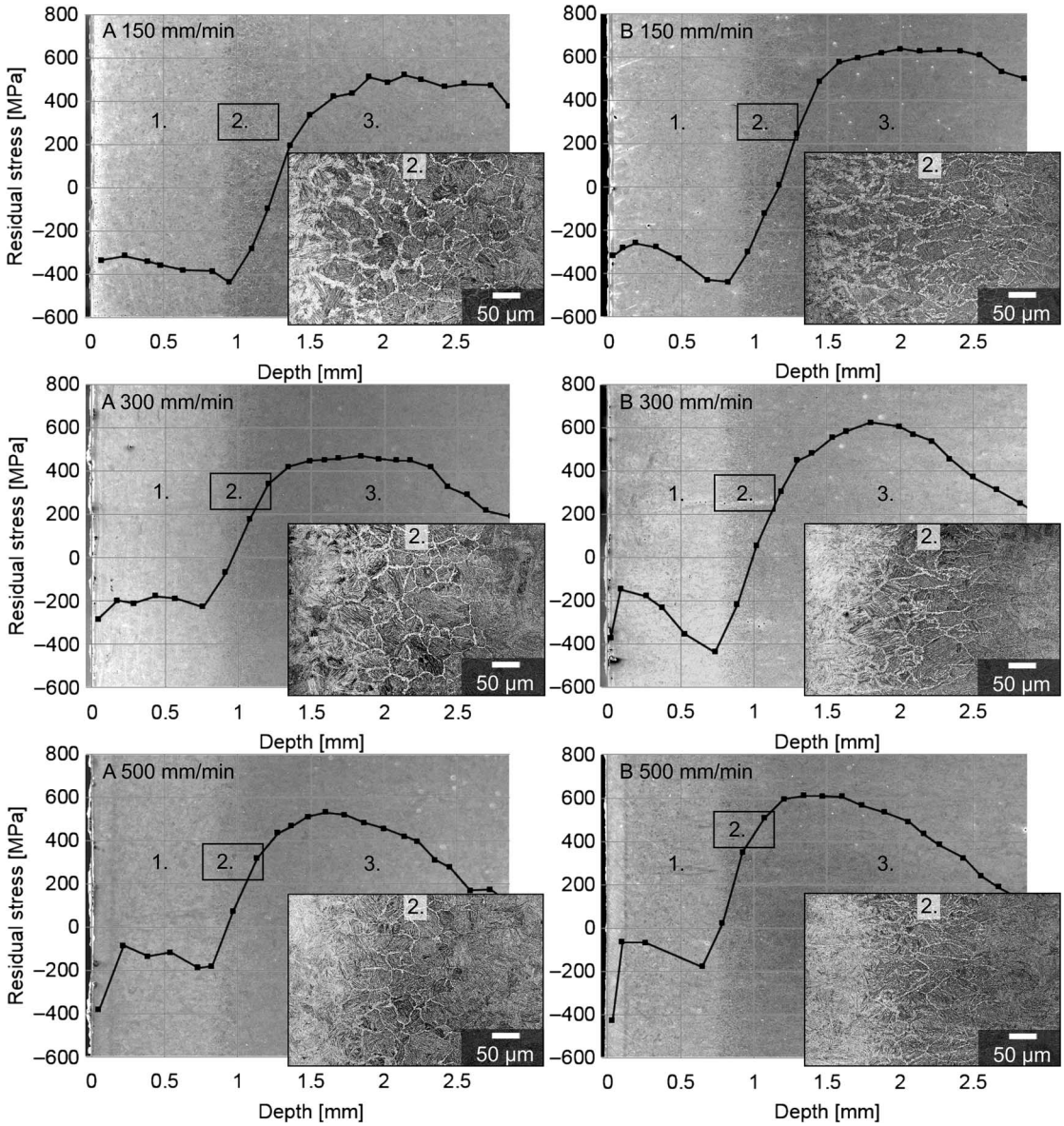

gradually decreases as it goes deeper into the subsurface. The fine structure of dispersed Fe_3C particles can be seen throughout the tempered region. The number of Fe_3C particles decrease deeper from the cut edge as the tempering of the structure decreases.

Microstructures of the cut edge and two-phase region are presented in Fig. 10 for specimens A and B after flame cutting was performed at speeds of 150, 300, and 500 mm/min. Additionally, Fig. 10 shows the measured RS profiles in the thickness direction for each specimen.

The microstructures of the flame-cut edges (Fig. 10) indicate that the newly formed martensite region (1.) is wider near the cut edge at slower cutting speeds. As the cutting speed increases, the thickness of the newly formed martensite layer decreases. The heat input is higher at slower cutting speeds and, for this reason, the fully austenized region reaches deeper into the subsurface compared to faster cutting speeds. Similar observations can be made for the two-phase regions (2.), which are presented in Fig. 10. The two-phase region is the widest at a cutting speed of 150 mm/min while a cutting speed of 500 mm/min produces the narrowest two-phase region. Additionally, the two-phase regions of the specimens highlight the prior austenite grain structure (martensite formation at the PAGBs) and similar observations can be made from both the two-phase region and the reconstructed EBSD images (Fig. 5). The two-phase regions of Steel A consist of prior austenite grains with equiaxed morphology, while the same regions of Steel B contain prior austenite grains with clearly elongated morphology. In addition, Fig. 10 plainly shows the generation of RSs in different microstructural regions of the cut edge. The martensite transformation occurring near the cut edge (1.) creates compressive stress. After that, the RS values start to increase and transform into tensile stress within the two-phase region (2.). The highest RS values are attained in the tempered region (3.).

The RS profiles shown in Fig. 10 are collected in Fig. 11 for further comparison. In flame cutting, the RSs are caused by the thermal shock (thermal stresses) and microstructural changes (transformation stresses) that are produced by the high temperatures and fast cooling during the cutting process.

As previously mentioned, martensite transformation creates a compressive stress region near the cut edge of the steel plates (Fig. 11). The extent and the values of the compressive stress region depend on the cutting speed. A slow cutting speed produces a wider compressive stress region (it shifts the tensile stress peaks deeper into the subsurface) and more compressive stress compared to faster cutting speeds. After the compressive stress region, the RS levels start to increase and finally form tensile stress peaks in the tempered region. As can be seen in Fig. 11, the tensile stress peaks generated in Steel A are smaller in comparison with Steel B. In Steel B (Fig. 11b), the tensile stress

FIG. 11 RS profiles (thickness direction) measured for steel specimens (a) A and (b) B at cutting speeds of 150, 300, and 500 mm/min.

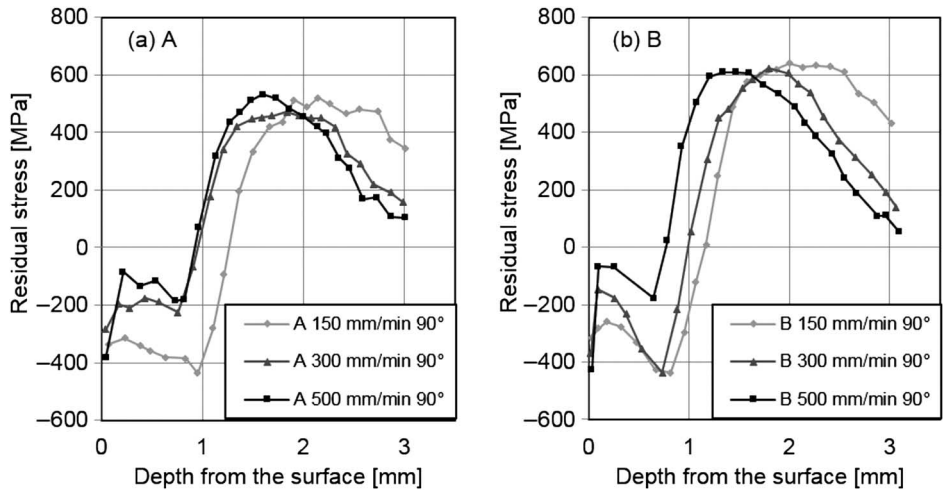

FIG. 12 Hardness profiles (HV 0.2 kg) from the cut edges of specimens (a) A and (b) B at cutting speeds of 150, 300, and 500 mm/min.

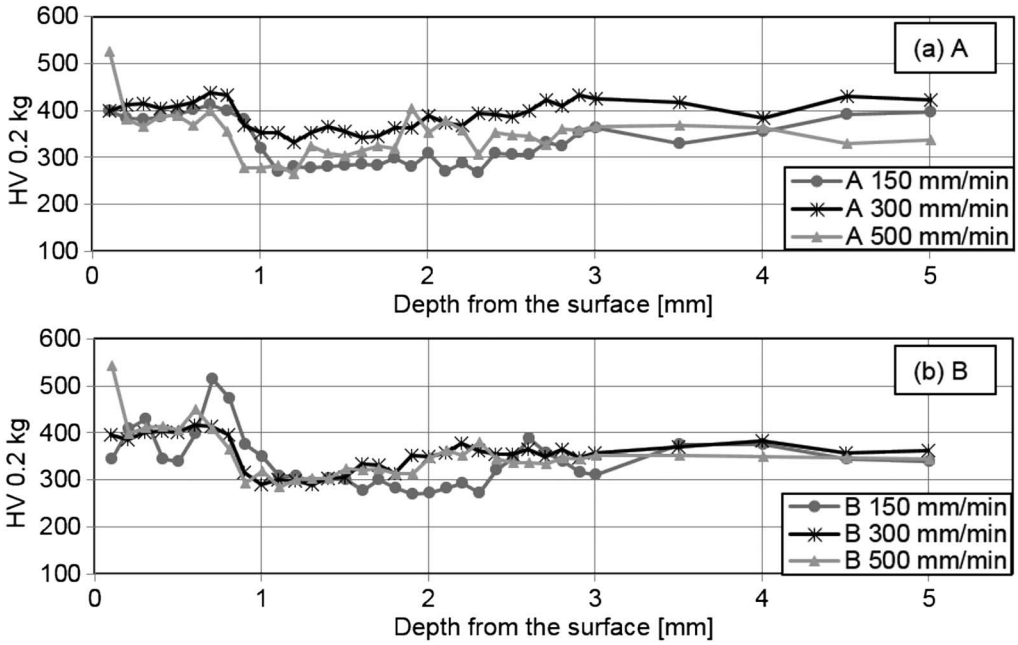

peak values are approximately 600 MPa in all the specimens. In contrast, the tensile stress peak values of Steel A (Fig. 11a) are approximately 100–150 MPa lower than in Steel B.

Fig. 12 presents the measured hardness profiles from the flame-cut edges of specimens A and B at cutting speeds of 150, 300, and 500 mm/min. The newly formed martensite region has the highest hardness levels near the cut edge in both steels. As the two-phase region starts, the hardness values gradually reduce as the content of newly formed martensite decreases and the fraction of tempered structure increases. The lowest hardness values are attained at the end of the two-phase structure where the original structure is the most tempered. After that, the hardness values start to increase toward the original hardness values. Fig. 12 indicates that the cutting speed has a role in determining the width of the area of the martensite region near the cut edge in both specimen materials. A faster cutting speed produces a narrower martensite region than slower cutting speeds. For this reason, hardness values start to decrease deeper in relation to the cut edge (as the two-phase region starts) at a cutting speed of 150 mm/min. In Steel A (Fig. 12a) there is some scatter in the hardness values in the tempered region and the 300 mm/min cutting speed shows higher values than those at cutting speeds of 150 and 500 mm/min. This might be due to segregation occurring in the hot rolling of the steel plates. Segregation can locally increase the hardness values and may create local hardness peaks in the hardness profiles. Similar hardness fluctuations can also be seen in Steel B, which is flame cut at 150 mm/min (Fig. 12b). The hardness changes from low (350 HV 0.2 kg) to high values (500 HV 0.2 kg) rapidly over a short distance.

GDOES profiles and SEM micrographs from the cut surfaces of Specimens. A and B are presented in Fig. 13. Both specimens were flame cut at a cutting speed of 300 mm/min. The GDOES profiles show that a thin iron oxide layer is formed in the cut surface during flame cutting. In addition, the cut surface is partly melted during the flame cutting process

FIG. 13

GDOES measurement and SEM micrographs from the cut surfaces of specimens (a) A and (b) B, which were flame cut using a cutting speed of 300 mm/min.

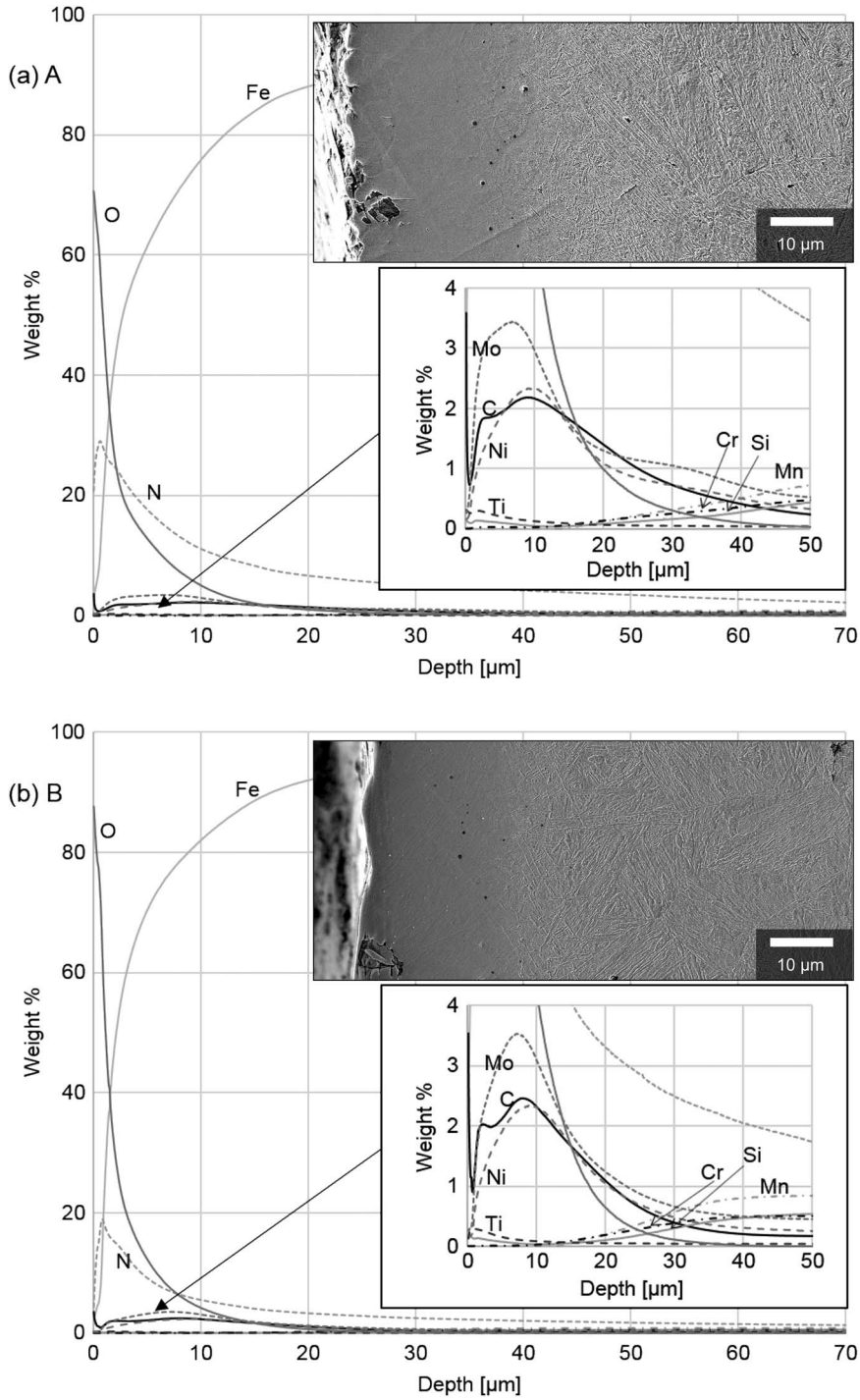

because of heat conduction and the molten region is enriched with carbon, molybdenum, and nickel. In addition, a small content of enriched titanium is present in the cut surface. However, results show that manganese, chromium, and silicon are burnt out from the cut

surface during the flame-cut process. A relatively high content of nitrogen, obtained in the cut surface, is most likely the result of diffusion from the atmosphere. The SEM micrographs in Fig. 13 show the partly molten surface region (grey areas in the cut surface without a clear microstructure). In general, the GDOES profiles from Specimen A and B are quite similar. The oxygen content near the cut edge is higher in Specimen B than in Specimen A. In contrast, the nitrogen level is lower in Specimen B compared to Specimen A.

The characterization of carbon extraction replicas was carried out for both as-received and flame-cut specimens. The carbon extraction replicas showed that both the original and the flame-cut specimens contained evenly distributed precipitates in the size range of 10–60 nm. The total investigated area was 136 μm^2 in each specimens. Steel specimen A contained 18 precipitates per 10 μm^2, Specimen B contained 17 precipitates per 10 μm^2, and flame-cut steel contained a similar amount of precipitates. This result indicates that precipitates were already formed during the manufacturing process and are not affected by flame cutting. The EDS analyses performed for individual precipitates indicate that they are titanium-rich precipitates. TEM micrographs and selected area electron diffraction (SAED) pattern of extraction replica specimen from steel A are presented in Fig. 14. SAED patterns indicate that the structure of the precipitates is a cubic rock salt structure (space group $Fm\bar{3}m$) which is a common structure for titanium carbides, titanium nitrides, and titanium carbonitrides (International Centre for Diffraction Data [ICDD], PDF-4+ 2015 database, 00-031-1400, 00-038-1420, 00-04201488).

After flame cutting, the specimens were inspected with ultrasound by two individual researchers, and the results are presented in Fig. 15. The ultrasonic inspection results clearly show that Steel B has a higher cracking tendency than Steel A. With the same amount of inspected cut surfaces (total cut edge length 4,800 mm), Steel A has 3 cracks (1 crack/1,600 mm) and Steel B has 14 cracks (1 crack/350 mm). The cracks located horizontally in the tempered region below the cut surface are according to the ultrasonic inspection results and the analysis of a few sectioned cracked specimens.

Discussion

Wear-resistant steel plates with two different microstructures were investigated to study the effect of microstructural features on the RS formation and cracking that was due to

FIG. 14

TEM analyses for the extraction replica specimen from Steel A. The amount of precipitates was not reduced or changed during flame cutting.

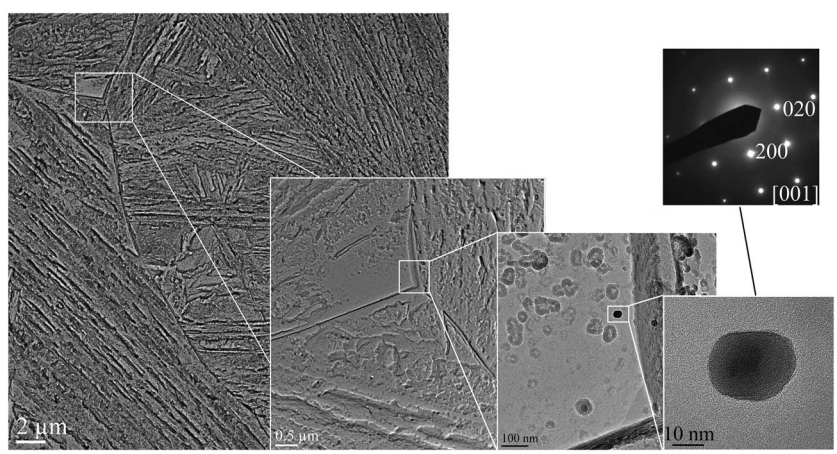

FIG. 15

Ultrasonic-inspected flame-cut specimens of Steels A and B.

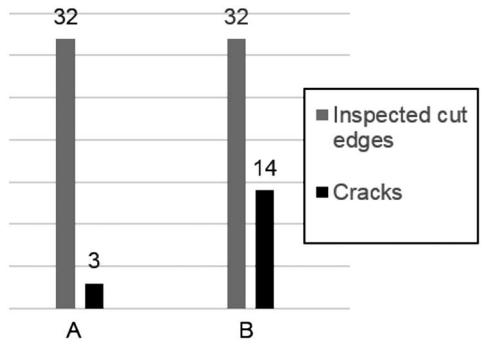

flame cutting. The chemical compositions and initial mechanical properties were approximately the same between the studied steels. As the microstructural analysis showed, the main difference in the studied steels was the prior austenite grain structure that was due to the different production histories. Steel A (equiaxed steel) consisted mainly of equiaxed prior austenite grains with few packet boundaries inside the grains, whereas the Steel B (elongated steel) contained elongated prior austenite grains in the horizontal direction with more packet boundaries. In addition, elongated steel had more block boundaries and a denser martensitic block structure compared to equiaxed steel. Generally, the martensite packet and block size are determined by prior austenite grains [19,20]. Additionally, the denser martensite blocks and packets in elongated steel compared to equiaxed steel may be caused by the bainite transformation that has taken place before martensite transformation. The formation of bainite refines subsequent martensitic packets and blocks, which has been reported [21] to increase the barriers to crack propagation. From the crack propagation point of view, it has been found [22] that existing boundaries in the martensitic structure are beneficial because they act as obstacles to crack propagation. Although both packet and block boundaries act as obstacles, it has been observed that packet boundaries deflect more cleavage cracks than block boundaries. The reason for this is the crystallographic misorientations of packet boundaries, which are bigger than block boundaries, and the fact that more energy is needed for the crack to cross packet boundaries. [22] However, PAGBs have been shown [19] to be the most effective barriers for crack propagation because they have a relatively high angle compared to other boundaries; in fact, a crack was observed to change direction as it encountered a PAGB. In the present study, the PAGS is larger in equiaxed steel than in elongated steel, which has more grain boundaries. However, the horizontally elongated PAGBs may act as potential paths for crack propagation rather than obstacles. Despite the bigger grain size, the equiaxed prior austenite grains would create more obstacles in the vertical direction in comparison with grain boundary chains as in elongated steel.

Flame cutting created three types of microstructural regions in the HAZ of the cut edge. A martensite region was formed closest to the cut edge. This region was fully austenized during flame cutting and, during cooling, formed martensite. After the martensite region, there was a two-phase region that partly austenized during flame cutting. The austenitization in the two-phase region occurred heterogeneously in the PAGBs, while the rest of the structure was tempered by the heat from the flame-cut process. After the

two-phase region, there was a tempered original structure in which the tempering effect gradually decreased as it went deeper into the subsurface. Generally, tempering is divided into four stages [23]. The first stage (<250°C) includes the redistribution of carbon atoms and precipitation of transition carbides such as ε ($Fe_{2.4}C$). However, it has been stated [24] that in low-alloy steels only the redistribution of carbon occurs in the first stage of tempering without ε-carbide formation. In the second stage (200°C–300°C), decomposition of retained austenite occurs. The third stage (200°C–350°C) involves the formation of Fe_3C particles, which most likely nucleate in ε-iron carbide interfaces and in both the interlath boundaries of martensite and the PAGBs. In the fourth stage (>350°C), Fe_3C particles coarsen and spheroidize. [23] However, in the present study, the tempering process could take place only for a very short time at high temperatures near the cut edge during flame cutting. The migration of trapped carbon atoms occurs within a short period of time. As the carbon content of the studied steel is low, it is assumed that ε-carbide precipitation does not occur. Fe_3C formation, in turn, starts as the temperature rises above 200°C. However, it seems that there is not enough time for any significant coarsening of Fe_3C particles, which leads to a fine, dispersed Fe_3C structure.

The martensite region had the highest hardness of all three regions; however, it started to decrease in the two-phase region. The lowest hardness values were in the tempered region, which followed the two-phase region, and after that, the hardness gradually increased deeper into the subsurface. According to Wood [5], the hardness of the surface region increases with faster cutting speeds. This was explained by the HAZ microstructures that were identified as a bainite with a slower cutting speed and as a martensite with a faster cutting speed. The present study shows that the hardness values in the surface region (>0.8 mm) were approximately the same with all studied cutting speeds. The reason for this is that the cooling conditions with all used cutting speeds produce similar kinds of martensite structures close to the cut edge.

According to a study by Lindgren, Carlestam, and Jonsson [7], flame cutting created a compressive or low tensile stress region (>1 mm) near the cut edge, which was followed by a tensile stress peak (2–3 mm below the surface). It was also stated that RS can be affected by chancing the cut parameters, for example, by using preheating. Similar results were also found in earlier studies by the current author [10,11], which state that the RS levels could be affected by using different cutting parameters, such as cutting speed. The present study shows that the shape of the RS profiles (compressive region near the cut edge followed by tensile stress peak) are similar to those in the previous studies [7,10,11]. In addition, it can be clearly seen how RS levels are chanced depending on the microstructural region in the HAZ. The martensite region produced residual compressive stress near the cut edge, and the RS changed from compressive to tensile stress in the two-phase region. The highest tensile stress values were in the tempered region following the two-phase region. As the cutting speed increases, the width of the martensite and two-phase region decreases because of the lower heat input created by the flame cutting process. In addition, a slower cutting speed produced more residual compressive stress in the cut edge compared to a faster cutting speed. According to the author's earlier study [11], the reason for this is that a fast cutting speed produces higher temperature differences in the cut edge during flame cutting compared to a slow cutting speed. The heating stage creates a thermal shock, which causes high thermal tensile stress (that is caused by uneven plastic strain due to the thermal expansion and contraction that occurs during flame cutting) close to the cut edge. The thermal shock is greater at faster cutting speeds and, for this reason,

produces more thermal tensile stress in the surface. During cooling, the austenized surface region forms martensite, leading to the structural expansion of the surface area, which is partly restrained by the inner structure. The expansion caused by martensite formation changes the thermal tensile stresses that are in the surface to compression stresses. As the thermal shock (and thermal tensile stress) is higher at faster cutting speeds, the martensite expansion creates less compressive stress in the surface region than it would at a slower cutting speed.

Equiaxed steel produced lower tensile stress peaks compared to elongated steel. In elongated steel, the tensile stress peak values are approximately 600 MPa in all the specimens. In contrast, the tensile stress peak values of equiaxed steel are approximately 100–150 MPa lower than in elongated steel. The RS results indicate that the microstructural features of equiaxed steel produce less tensile stress in the cut edge compared to elongated steel. Studies have shown [25] that dislocation pileups exist in the vicinity of grain boundaries and affect the local RS levels. A dislocation pileup creates a local stress peak in the grain boundary, and the RS levels monotonically decrease with increasing distance from the grain boundary. Elongated steel has more high-angle grain boundaries present in the vertical direction compared to equiaxed steel, which might create local stress peaks in the structure. In addition, the elongated shape of the grains indicate that the structure contains more dislocations in comparison with equiaxed prior austenite grains. As a result, the local stress peaks that are formed in the grain boundary level (Type II RS) may be superimposed in the measured RS profiles (Type I RS) thus creating higher tensile stress levels in elongated steel compared to equiaxed steel.

The ultrasonic inspection results showed that elongated steel contained more cracks than those contained in equiaxed steel. The cracks were located in the tempered region below the cut surface, which also contained the highest residual tensile stresses. These results indicate that the combination of high residual tensile stress with the microstructural features observed from elongated steel led to an enhanced cracking tendency in comparison with equiaxed steel. The results of this study indicate that the horizontally elongated grain structure is unbeneficial in both RS and crack formation points of view. The elongated prior austenite grain–structured steel produced higher tensile stress peaks during flame cutting compared to steel, which consisted of equiaxed prior austenite grains. In addition, elongated prior austenite grain structures create long parallel grain boundary chains, which can act as possible paths for crack formation. The susceptible microstructure of elongated prior austenite grains associated with the high residual tensile stresses formed during flame cutting make the steel plate vulnerable to crack formation.

Conclusions

Wear-resistant steel plates with two different microstructures were investigated to study the effect of microstructural features on the RS formation and cracking that is due to flame cutting. The following conclusions can be made from this study:

(1) The flame cutting process creates three types of microstructural regions in the HAZ of the cut edge: the martensite region, two-phase region, and tempered original structure. The depth of these regions was shown to depend on the cutting speed.

(2) Different microstructural regions have different hardness and RS values. The martensite region closest to the cut edge is the hardest and tends to produce compressive RS. In the two-phase region, the hardness values decrease, and RS values start to increase as the newly formed martensite region is mixed with the tempered original structure. The original structure, which is tempered during the flame cutting process, has both the lowest hardness values and the highest residual tensile stress values.
(3) Equiaxed prior austenite grains produced lower tensile stress peaks compared to steel with horizontally elongated prior austenite grains.
(4) Elongated prior austenite grain–structured steel was more prone to cracking compared to equiaxed steel. Horizontally elongated PAGBs can act as potential paths for crack propagation. Equiaxed prior austenite grains created more obstacles in the vertical direction in comparison with grain boundary chains found in elongated prior austenite grain structures.
(5) Prior austenite grain structures have an effect on both the RS formation and the probability of cracking. The combination of elongated prior austenite grains and high-residual tensile stresses makes steel plates more prone to crack formation during the flame cutting process.

ACKNOWLEDGMENTS

The funding for this work was mainly provided by the Tampere University of Technology graduate school. The authors would like to thank Mr. Petri Jussila (SSAB) for carrying out the GDOES experiments.

References

[1] Soisson, L. R., "Oxyfuel Gas Cutting," *ASM Handbook Volume 6: Welding, Brazing, and Soldering*, ASM International, Materials Park, OH, 1993, pp. 1155–1165.
[2] Thiébaud, R., Drezet, J., and Lebet, J., "Experimental and Numerical Characterisation of Heat Flow during Flame Cutting of Thick Steel Plates," *J. Mater. Process. Technol.*, Vol. 214, No. 2, 2014, pp. 304–310, https://doi.org/10.1016/j.jmatprotec.2013.09.016
[3] Martín-Meizoso, A., Aldazabal, J., Pedrejón, J. L., and Moreno, S., "Resilience and Ductility of Oxy-Fuel HAZ Cut," *Frattura ed Integrita Strutturale*, Vol. 30, 2014, pp. 14–22.
[4] Wilson, A. D., "Hardness Testing of Thermal Cut Edges of Steel," *Eng. J. Am. Inst. Steel Constr.*, Vol. 27, No. 3, 1990, pp. 98–105.
[5] Wood, W. E., *Heat-Affected Zone Studies of Thermally Cut Structural Steels, Report No. FHWA-RD-93-015*, Federal Highway Administration, McLean, VA, 1994, 92p.
[6] HARDOX TechSupport, SSAB Oxelösund, Stockholm, Sweden, 2007, 2p, http://www.aemach.com/hardox/pdf/016_TS_Hardox_Cutting_of_Hardox_wear_plate_UK.pdf
[7] Lindgren, L., Carlestam, A., and Jonsson, M., "Computational Model of Flame-Cutting," *J. Eng. Mater. Technol.*, Vol. 115, No. 4, 1993, pp. 440–445, https://doi.org/10.1115/1.2904243
[8] Withers, P. and Bhadeshia, H., "Residual Stress. Part 1—Measurement Techniques," *Mater. Sci. Technol.*, Vol. 17, No. 4, 2013, pp. 355–365, https://doi.org/10.1179/026708301101509980
[9] Withers, P. and Bhadeshia, H., "Residual Stress. Part 2—Nature and Origins," *Mater. Sci. Technol.*, Vol. 17, No. 4, 2013, pp. 366–375, https://doi.org/10.1179/026708301101510087
[10] Jokiaho, T., Saarinen, T., Santa-Aho, S., Peura, P., and Vippola, M., "The Characterization of Flame Cut Heavy Steel—The Residual Stress Profiling of Heat Affected Surface Layer," *Key Eng. Mater.*, Vol. 674, 2016, pp. 103–108, https://doi.org/10.4028/www.scientific.net/KEM.674.103

[11] Jokiaho, T., Laitinen, A., Santa-aho, S., Isakov, M., Peura, P., Saarinen, T., Lehtovaara, A., and Vippola, M., "Characterization of Flame Cut Heavy Steel: Modeling of Temperature History and Residual Stress Formation," *Metall. Mater. Trans. B*, Vol. 48, No. 6, 2017, pp. 2891–2901, https://doi.org/10.1007/s11663-017-1090-x

[12] EN 15305, *Non-Destructive Testing—Test Method for Residual Stress Analysis by X-Ray Diffraction*, German Institute for Standardization, Berlin, Germany, 2008, https://standards.globalspec.com

[13] Fitzpatrick, M., Fry, A., Holdway, P., Kandil, F., Shackleton, J., and Suominen, L., *Determination of Residual Stresses by X-Ray Diffraction, Measurement Good Practice Guide No. 52*, National Physical Laboratory, Teddington, UK, 2005, 77p.

[14] SFS-EN ISO 6892-1, *Metallic Materials—Tensile Testing—Part 1: Method of Test at Room Temperature*, Finnish Standards Association, Helsinki, Finland, 2016, www.iso.org

[15] Nyyssönen, T., Isakov, M., Peura, P., and Kuokkala, V.-T., "Iterative Determination of the Orientation Relationship between Austenite and Martensite from a Large Amount of Grain Pair Misorientations," *Metall. Mater. Trans. A*, Vol. 47, No. 6, 2016, pp. 2587–2590, https://doi.org/10.1007/s11661-016-3462-2

[16] Bachmann, F., Hielscher, R., and Schaeben, H., "Texture Analysis with MTEX—Free and Open Source Software Toolbox," *Solid State Phenom.*, Vol. 160, 2010, pp. 63–68, https://doi.org/10.4028/www.scientific.net/SSP.160.63

[17] Järvinen, H., Isakov, M., Nyyssönen, T., Järvenpää, M., and Peura, P., "The Effect of Initial Microstructure on the Final Properties of Press Hardened 22MnB5 Steels," *Mater. Sci. Eng., A*, Vol. 676, 2016, pp. 109–120, https://doi.org/10.1016/j.msea.2016.08.096

[18] Rudnev, V., Fett, G. A., and Semiatin, S. L., "Tempering of Induction-Hardened Steels," *ASM Handbook Volume 4C: Induction Heating and Heat Treatment*, ASM International, Materials Park, OH, 2014, pp. 130–159.

[19] Li, S., Zhu, G., and Kang, Y., "Effect of Substructure on Mechanical Properties and Fracture Behavior of lath Martensite in 0.1C–1.1Si–1.7Mn Steel," *J. Alloys Compd.*, Vol. 675, 2016, pp. 104–115, https://doi.org/10.1016/j.jallcom.2016.03.100

[20] Zhang, C., Wang, Q., Ren, J., Li, R., Wang, M., Zhang, F., and Sun, K., "Effect of Martensitic Morphology on Mechanical Properties of an As-Quenched and Tempered 25CrMo48V Steel," *Mater. Sci. Eng., A*, Vol. 534, 2012, pp. 339–346, https://doi.org/10.1016/j.msea.2011.11.078

[21] Zhou, T., Yu, H., and Wang, S., "Effect of Microstructural Types on Toughness and Microstructural Optimization of Ultra-Heavy Steel Plate: EBSD Analysis and Microscopic Fracture Mechanism," *Mater. Sci. Eng., A*, Vol. 658, 2016, pp. 150–158, https://doi.org/10.1016/j.msea.2016.02.001

[22] Wang, C., Wang, M., Shi, J., Hui, W., and Dong, H., "Effect of Microstructural Refinement on the Toughness of Low Carbon Martensitic Steel," *Scr. Mater.*, Vol. 58, No. 6, 2008, pp. 492–495, https://doi.org/10.1016/j.scriptamat.2007.10.053

[23] Bhadeshia, H. and Honeycombe, R., "The Tempering of Martensite," *Steels: Microstructure and Properties*, 3rd ed., Butterworth-Heinemann, Oxford, 2006, pp. 183–208.

[24] Jack, D. H. and Jack, K. H., "Invited Review: Carbides and Nitrides in Steel," *Mater. Sci. Eng.*, Vol. 11, No. 1, 1973, pp. 1–27, https://doi.org/10.1016/0025-5416(73)90055-4

[25] Basu, I., Ocelík, V., and De Hosson, J. T. M., "Measurement of Spatial Stress Gradients Near Grain Boundaries," *Scr. Mater.*, Vol. 136, 2017, pp. 11–14, https://doi.org/10.1016/j.scriptamat.2017.03.036